Targeted Imaging of Orthotopic Prostate Cancer by Using Clinical Transformable Photoacoustic Molecular Probe

Chen Qiu
 the 3rd Affiliated Hospital of Sun Yat-sen University

Tinghui Yin
 The 3rd Affiliated Hospital of Sun Yat-sen University

Yuanyuan Bai
 Shenzhen Institutes of Advanced Technology Chinese Academy of Sciences

Xiaoyan Miao
 The 3rd Affiliated Hospital of Sun Yat-sen University

Rongkang Gao
 Shenzhen Institutes of Advanced Technology Chinese Academy of Sciences

Huichao Zhou
 The 3rd Affiliated Hospital of Sun Yat-sen University

Ren Jie
 The 3rd Affiliated Hospital of Sun Yat-sen University

Liang Song
 Shenzhen Institutes of Advanced Technology Chinese Academy of Sciences

Chengbo Liu
 Shenzhen Institutes of Advanced Technology Chinese Academy of Sciences

Hairong Zheng
 Shenzhen Institutes of Advanced Technology Chinese Academy of Sciences

Rongqin Zheng (✉ zhengrq@mail.sysu.edu.cn)

Research article

Abstract

Background: To obtain high yield histological samples by targeted PCa biopsy is the current trend compared of transrectal ultrasound (TRUS) guided systematic histological biopsy which is regarded as golden standard for prostate cancer (PCa) diagnosis. In this paper, we present a targeted PCa imaging strategy using real-time molecular photoacoustic imaging system integrated with handheld US probe (PAI/US) and synthesized integrin αvβ3 targeted probe based on ICG (cRGD–ICG). Results: A small molecular PAI probe was synthesized and proved excellent targeted imaging ability in vitro. In vivo photoacoustic imaging was carried out after intravenous injection of cRGD-ICG in orthotopic PCa bearing beard rats under facilitation of PAI/US system. Maximum molecular photoacoustic signals were observed in the tumor area in vivo post probe injection, which showed 3.8 folds higher signal enhancement than in the control group (P < 0.05, respectively). Significant higher cRGD-ICG accumulation was observed under confocal microscopy in tumor region rather than normal prostate tissue. Conclusions: All our results showed that the comprehensive strategy provided a high-yield and reliable method for PCa diagnosis and targeted prostate biopsy, with great clinical transforming potential.

1. Background

Prostate cancer (PCa) is the second most common malignancy and is the leading cause of death among the tumor-onset male population worldwide[1−3]. Universally, systematic histological biopsy guided by transrectal ultrasound (TRUS) has been regarded as the goldern standard procedure for diagnosing PCa[4]. However, since sensitivity and specificity of US method to identify the malignancies is relatively low, the US is mainly used for providing anatomical references within prostate while performing a systemic biopsy. Besides, the systemic biopsy is user dependent and may results in inconsistent sampling [5], which often leads to missing clinically significant prostate. Thus, to overcome the limitations of systematic biopsy, targeted biopsy techniques are being explored of which multiparametric Magnetic Resonance Imaging (mpMRI) is the most commonly used [6]. In the mpMRI technique, suspicious regions identified in MRI are targeted for biopsy under US guidance using fusion imaging. However this technique alone is unable to obtain real-time guidance for biopsy and still too expansive to afford which has 5−15% false-negative cancer detection rate[7]. Therefore it is limited by the detectability of PCa targeted biopsy.

US molecular imaging is also a complementary tool to enhance the accuracy of PCa diagnosis while using US. A first-in-human US molecular imaging trial with BR55 as a vascular endothelial growth factor receptor 2-targeted contrast agent has shown promise for specific detection of human PCa [8]. However, since the missed lesions rate is as high as 32%, it still cannot be used clinically and its feasibility for diagnosing PCa needs to be further explored [8]. Thus, it remains a challenge to search for an imaging modality reliably distinguishing benign from malignant tissue of prostate for improved PCa detection [9].

Photoacoustic imaging (PAI) is an emerging clinical modality that combines high sensitivity inherent to optical properties, as deep as 5 cm, and high spatial resolution inherent to US imaging [10]. The

photoacoustic imaging system can be easily integrated into the clinical US imaging platform without degrading the inherent US imaging capability. Hence the PAI modality has provided unprecedented opportunities for PCa diagnosis. Both preclinical and clinical researches have already demonstrated the ability of PAI for localizing tumors[11−13]. Furthermore, as in other mainstream imaging modalities such as in US, CT or MRI, the tumor cells can also be pre-labeled with photoacoustic molecular probes for contrast-enhanced imaging. The combination of PAI and molecular probe targeting and labeling, also called as photoacoustic molecular imaging, has shown great potential to identify malignances, including PCa. Few studies with molecular PAI have already been performed to identify PCa, especially in orthotopic PCa models, which mimic the heterogeneous tumor microenvironment, foretelling the feasibility of clinical transformation[14].

For molecular PAI, exogenous contrast agents including nanoparticles and dyes are commonly used for providing sufficient contrast in the signal. Specifically, small molecular dye indocyanine green (ICG) has great translational potential for clinical PAI because of high biosafety level. The ICG is a near-infrared fluorescent dye already approved by the US Food and Drug Administration (FDA) for clinical imaging applications[15]. Consequently, ICG is currently used with PAI clinically, such as identifying the sentinel lymph node, which is critical for cancer staging[11]. However, free ICG has several drawbacks for in vivo imaging, including a tendency to aggregate, instability in aqueous solution, rapid clearance from the bloodstream, and lack of targeting abilities[16−17]. Thus, ICG combined with stable and targeted molecular probes are needed for PCa, since free ICG alone cannot be used for targeting PCa with PAI.

The cell adhesion molecule integrin $\alpha_v\beta_3$ is known to play a critical role in angiogenesis and metastasis in several tumor types including PCa by significantly up-regulating active endothelial cells and fast-growing solid tumor cells[18−19]. The molecular probes linking RGD, namely arginine-glycine-aspartic acid sequence, with $\alpha_v\beta_3$ integrin receptor would enable noninvasive monitoring of tumor angiogenesis and metastasis using PAI[20]. This ICG-based molecular probe would be an ideal candidate for PCa management with PAI.

The current study we present a photoacoustic molecular imaging-based technique to identify malignancies by enhancing both functional and molecular information of PCa using a synthesized molecular probe to increase the detectability of the prostate cancer for better US-based targeted prostate biopsy, overcoming the limitations of previous targeted methods [21−22].

2. Methods

2.1 Synthesis and Characterization of cRGDyk Conjugated ICG

cRGD-ICG Synthesis. Monomeric cyclic RGD peptide c(RGDyK) was used (Shangon, Shanghai) for the synthesis of the probe. Appropriate c(RGDyK) was mixed with ICG-NHS ester (Kaixin, China) in the molar

ratio of 1:3 by dissolving in dimethyl sulfoxide (DMSO). The reaction mixture was incubated for 4 h in the dark at room temperature. Subsequently, the mixture was expanded to 3 ml solution by adding water. The solution was then transferred to a dialysis device for 48 h at 4 °C to exceed free ICG. The concentrated c(RGDyK)-ICG solution was finally lyophilized to remove organic solvents. Finally, the powder of c(RGDyK)-ICG was dissolved in water and stored at -20 °C in the dark until used. Brief procedures describing cRGD-ICG synthesis are shown in Fig. 1. The synthesized cRAD-ICG was made as negative control via linking ICG to the non-functional cRAD peptide.

Characterization of cRGD-ICG. Ultraviolet-Visible (UV-Vis) spectra and fluorescence spectra of the probes were obtained by using a UV-Vis spectrophotometer (Evolution 220, Thermo Scientific) and a fluorescence spectrophotometer (Lumina, Thermo Scientific), respectively. In vitro photoacoustic imaging of the probes was performed using a handheld US linear array-based photoacoustic imaging system (Shenzhen Institutes of Advanced Technology, Chinese Academy of Sciences, Shenzhen). A series of different concentration probes (1.25-20 µg/ml) were placed in 96-well plates by adding 200 µl solution to each well. Further quantitative photoacoustic signal of the probe was obtained using MATLAB software.

2.2 Cell Culture

Human Umbilical Vein Endothelial Cells (HUVEC) expressing $\alpha_v\beta_3$ integrin and human embryonic kidney cells (293T) barely expressing integrin $\alpha_v\beta_3$ were purchased from the Cell Bank of Shanghai Institutes for Biological Sciences, Chinese Academy of Sciences (Shanghai, China). Both cell lines were grown in DMEM containing 10% fetal bovine serum (FBS) at 37 °C in a humidified atmosphere with 5% CO_2. When the cells reached 70% confluence, they were trypsinized and subcultured. All cell culture reagents were obtained from Invitrogen Corporation (Carlsbad, CA, USA). Cells were seeded in 6-well plates at a density of 1×10^5 cells per well and were incubated overnight in complete cell growth medium. The 0.5 ml medium containing either cRGD-ICG or cRAD-ICG was incubated with the cells for 1 h at 37 °C. The medium was then changed back to complete cell growth medium for normal cell culture before conducting binding affinity experiments.

2.3 Cell Specific Uptake of cRGD-ICG Assay

To examine the intracellular uptake of cRGD-ICG or cRAD-ICG, both HUVEC and 293T were incubated with either cRGD-ICG or cRAD-ICG (20 µg/ml) for 1 h at 37 °C. After incubation, unbound dyes were removed with a gentle PBS wash and the media was replaced before imaging. On the obtained final solution, flow cytometry (Accuri C6, BD, USA) was performed to determine quantitative binding through the ICG signal.

Cells also went through a similar procedure to test for cellular targeting ability of PAI. Once cell solutions were collected, they were subcutaneously injected into the backside of a normal murine model and were observed with a photoacoustic system (Shenzhen Institutes of Advanced Technology, Chinese Academy of Sciences). Further quantitative data was obtained using MATLAB software offline.

2.4 Murine Model of Orthotopic Prostate Cancer

All animal experiments were approved by the Sun Yat-sen University Animal Care Committee. All experimental rats were purchased from Charles River (Beijing, China). A male nude rat (Sprague Dawley Rat) bearing orthotopic xenografted PCa model was established. The operation procedures were as follows: 12 matured rats weighing 250–300 g were used for the study. All rats were kept in a temperature and humidity-controlled room and were divided into 2 groups randomly: cRGD-ICG and cRAD-ICG group (n = 6 of each group). The rats were fasted 18 h before the operation but were fed chow and water. The experiment began after they were appropriately anesthetized by injecting pentobarbital sodium (30 mg/kg, i.p.). Then longitudinal incisions were made in the lower abdomen to expose the prostate. A 50 µl human prostatic carcinoma cell lines (PC-3) suspension of 5×10^6 / ml were then injected into the gland. The incision in the abdomen was closed, and successful orthotopic PCa modeling was confirmed 3 days after the operation by pathology (Further details are provided in the supplemental materials and methods).

2.5 In vivo PAI Molecular Imaging

Rats in each group were injected with 200 µl cRGD-ICG or cRAD-ICG (50 µg/ml) solution via tail vain. Imaging was performed at a series of time points after injection: 0 h, 5 min, 2 h, 4 h, 8 h, 12 h. We used PAI/US dual-modality imaging system with the following details: 7 MHz transducer, lateral and axial resolution of 336 and 235 µm respectively, 15 mJ/cm^2 laser fluence, 795 nm wavelength, 6 ns laser pulse width, 20 Hz pulse repetition frequency. Further details of the imaging system used can be found in our previous publications[21–22]. The transducer surface was maintained at about 9 mm from the surface of the skin and is coupled with clear and colorless US gel for uniform light illumination to the gland and for consistent imaging between different time points. B-mode US images were used as a reference to maintain consistent imaging planes between different imaging time points and for general anatomy information.

2.6 Analysis of In vivo PAI Imaging Data

We quantified the integrin $\alpha_v\beta_3$ targeted PAI signal using MATLAB-based algorithm. The engineer was blinded to group assignment and outcome. The co-registered B-mode US images were used as a guidance to select the region of interest (ROI) in the prostate gland comprising both normal and cancerous tissues. Within the identified ROI, PAI signal identifying PCa tissues were analyzed. The quantitative PAI signal was presented as the ratio of pixels containing molecular signal post-injection compared to the signal pre-injection. In addition, absolute quantitative PAI signals at each point of imaging depth were also calculated.

2.7 Histological Confirmation of ICG Localization in Murine Prostate Cancer

After 12 h post-injection, animals were euthanized by injecting excessive pentobarbital sodium 100⍰150mg⍰kg. Afterwards the whole prostate including tumor was resected and frozen in optimal cutting temperature (O.C.T.) for pathology (see details in supplemental materials and methods). A

confocal laser scanning microscope imager (Leica, Germany) was used to acquire fluorescent images of tissue sections. The ICG component in the molecular probe can be seen in both photoacoustic images in vivo as well as in fluorescence image of tissue sections. The pathology of suspicious accumulation of cRGD-ICG region, identified as PCa in the real-time PAI imaging, was confirmed by pathology result. Tissue sections (10 µm thickness) of two groups were rinsed in PBS for 5 min to remove O.C.T. and then fixed for 5 min in 4% PFA. Slides were then imaged using PA at 405 nm for the nuclei and 633 nm for ICG.

2.8 Statistical Analysis

All experiments were repeated 3 times, and the data were analyzed using Student's t-tests and one-way ANOVA analysis (SPSS software, version 13.0, SPSS Inc.). Unless otherwise specified, data were expressed as the means ± standard deviation. A two-sided P-value of less than 0.05 was considered indicative of a statistically significant difference in values.

3. Results

3.1 Synthesis and Characterization of cRGD-ICG

As described before, brief procedures of c(RGDyK)- ICG synthesis by amide linkage are shown in Fig. 1. NHS ester reacted with theε-amino group of the lysine residue of the RGD peptides.

In buffer, as shown in Fig. 2A and 2B, the fluorescence emission and absorption characteristics of the targeted cRGD based dyes and non-targeted dyes were similar. The maximum emission of light for cRGD-ICG is at 799 nm (Fig. 2A), and the specific absorption wavelength of cRGD-ICG is at 795 nm (Fig. 2B), where PAI imaging will be optimum. At 795 nm, in vitro PAI properties of the molecular probe were tested with different concentrations range (1.25-20 µg/ml) and results are shown in Fig. 2C and 2D. The cRGD-ICG displayed a stable linear PAI signal increase as the concentration was increased linearly from 1.25 to 20 µg/ml.

3.2 Cell specific uptake of cRGD-ICG assay

To examine the binding affinity of cRGD-based probes towards the integrin $\alpha_v\beta_3$ receptor in vitro, we tested both HUVECs cell lines and 293T cell lines (as control). After incubating 50% of HUVECs with a targeted agent (cRGD-ICG) and other 50% with a non-targeted agent (cRAD-ICG), cells were collected for flow cytometry. As shown in Fig. 3, HUVECs with abundant integrin $\alpha_v\beta_3$ receptors expressed much stronger ICG signal when incubated with cRGD-ICG compared to those incubated with cRAD-ICG. The quantitative analysis showed that the binding efficacy of cRGD-ICG toward HUVECs was 93.8 ± 5.7% (P > 0.05), which confirmed the excellent targeting ability of cRGD-ICG laying the foundation for in vivo molecular imaging. In control cell groups, 293T cells with very low expression of integrin $\alpha_v\beta_3$ receptors barely displayed ICG signal when incubated with cRGD-ICG or cRAD-ICG. In addition, the difference of cellular uptake for 293T cells had no statistical significance between cRGD-ICG and cRAD-ICG (P < 0.05).

We then conducted live-cell PAI using the same cell lines to verify cellular targeting ability. Cells incubated with probes were injected subcutaneously into the dorsal side of a murine model to facilitate PAI. As shown in Fig. 4, HUVECs belonging to the cRGD-ICG group showed significant PAI signal while those belonging to the cRAD-ICG group showed very low PAI signal (Fig. 4A). The 293T cells, independent of the targeted or non-targeted probe, showed very low molecular signals. The quantitative analysis (Fig. 4B) showed that the HUVECs belonging to the cRGD-ICG achieved almost 2.4x enhanced PAI signal intensity compared to the control groups (P < 0.05). This demonstrates the targeting ability of the cRGD-ICG at a cellular level for enhanced PAI imaging.

3.3 Dynamic molecular PAI of cRGD-ICG in orthotopic prostate cancer in vivo

The successful murine orthotopic prostate tumor model is shown in Fig. S1 and the tumor sections collected to confirm the expression of integrin $\alpha_v\beta_3$ is shown in Fig. S2. To assess the feasibility of using the $\alpha_v\beta_3$ molecular probe for murine orthotopic PCa targeting, cRGD-ICG was injected into 6 rats via tail vein. The cRAD-ICG was injected into the remaining 6 rats and was used as a negative control probe. The PAI was performed at a series of time points before and after probe injection to better understand the physiological behavior of cRGD-ICG. The PAI imaging of the abdominal region of the murine models was performed with rats laying on their dorsal size and transducer placed anteriorly. The maximum amplitude projection images of one of the rat's abdomen are shown in Fig. 5. In the top row of Fig. 5, it can be seen that the cRGD-ICG accumulated temporally (for 12 h post probe injection) and spatially at suspicious tumor area in the prostate. The malignancy of the tumor area was further confirmed by pathology (Fig. 7). Other rats within the cRGD-ICG group showed a similar tendency as shown in the left column of Fig. S3. For the control rats injected with cRAD-ICG, no obvious probe accumulation occurs in the prostate tumor area as shown in the bottom row of Fig. 5 and the right column of Fig. S3.

3.4 Molecular PAI/US of orthotopic prostate cancer

The molecular PAI/US imaging was performed at optimum imaging time (12 h post probe injection) to identifying PCa. As shown in Fig. 6A, PAI images show integrin $\alpha_v\beta_3$ molecular signal merged with B-mode US image providing valuable anatomical information around the tumor. The rats injected with cRGD-ICG showed significant molecular PAI signal enhancement at orthotopic tumor area 12 h post injection with the US showing the surrounding tumor structures (Fig. 6A). In the rats injected with cRAD-ICG, only sparse molecular PAI signal distribution was observed in the same region (Fig. 6A). The prostate area with PCa showed an average of 5.1x increase in molecular PAI signal while only 1.3x in the control group post probe injection (P < 0.05, respectively) compared to baseline pre-injection signal (Fig. 6C). The quantitative PAI signals at different depths, from the skin to deep tissues, were also measured to check the location of maximum PAI signal. As expected, PAI signals of cRGD-ICG group peaked at a depth of 10 mm, which was the orthotopic PCa area (Fig. 6D).

The prostate tissues, including tumor area, were excised 12 h post injection for ex vivo PAI (Fig. 6B). In a cRGD-ICG group, $\alpha_v\beta_3$ molecular PAI signal was confirmed to accumulate mostly in the tumor region with

no significant signal accumulation in the normal prostate region (Fig. 6B). In a cRAD-ICG group, the whole prostate tissues, including tumor region, showed low PAI signal.

3.5 Histological Confirmation of ICG Localization in Murine Prostate Cancer

To confirm the accumulation of the probes within tumor tissues, the prostate cancer regions were excised 12 h post dyes injection for frozen slices. The cRGD-ICG and cRAD-ICG were visualized in the frozen slices using a confocal microscope to acquire fluorescence signals from ICG. The neovascularization's within the tumors were labeled with red fluorescence. As expected, abundant ICG signals (green color in the image) distributed along tumor neovascularization in the cRGD-ICG group were detected (Fig. 7). This result using microscope confirms the binding affinity of cRGD-ICG to neovascularization of PCa for targeting. For cRAD-ICG control group in vivo, ICG was barely found adhering to the vessels due to poor targeting ability of the probe.

4. Discussion

Systematic biopsy for prostate cancer detection, which is currently a golden standard to evaluate PCa, suffers from several limitations including low accuracy, uneven sampling, which can lead to under-sampling of clinically significant prostate cancer under diagnosis, and complications. As presented in the introduction, mpMRI and molecular US imaging are investigated for targeted biopsy to improve the efficiency of the core biopsy but have limitations [7, 8]. How to improve the targeting ability during image-guided biopsy remains a challenging issue. On the other hand, even though conventional US only aid in providing anatomical information of the prostate, the real-time convenience and reproducibility still make it valuable guidance tool. In addition, the general anatomical information provided by the US between the prostate and surrounding tissues, such as bladder and urethra, helps in reducing procedure injury. Therefore, the optimal way to address the targeted prostate biopsy is to find a targeting method that is complementary to US imaging, while increasing the success of the prostate biopsy.

The PAI system integrated with the US system provides such an opportunity to improve the efficacy of prostate biopsy. The photoacoustic molecular imaging compliments US imaging since it enables monitoring of the disease process with additional molecular and functional information in addition to providing anatomical structural information. The PAI is more accurate in distinguishing malignancies as reported in several literatures [11–13]. The PAI system can be easily integrated into the clinical US imaging platform without degrading the inherent US performance as reported in[].The fastest-growing molecular PAI overcomes the sensitivity limitation inherited from the US and has an excellent resolution at a satisfactory imaging depth for targeted PCa application.

In this study, we presented a molecular PAI targeting of PCa using a synthesized ICG, an FDA approved small molecular dye. Targeting substances such as peptide and proteins linked to the dye have been tried in the past to achieve targeting ability. In fact, proteins (for example, monoclonal antibodies) could

achieve higher targeting affinity and specificity compared to the peptide used in this study, but have poorer tissue penetration and clearance due to their larger size hindering their wider application. Thus, the molecular probe synthesized in this study showed greater clinical transforming ability.

A few other studies have focused on molecular PAI to detect PCa. Ni et al. monitored PCa growth in an orthotopic mouse model through the 3D US assisted PAI functional imaging by evaluating the angiogenesis feature of the tumor instead of molecular information [14]. Another similar study by Jelena et al. evaluated the utility of targeted PAI for PCa via a subcutaneous xenograft tumor model of nude mice[23]. In the present study, an orthotopic xenografted tumor model beard on rats was used instead of the subcutaneous tumor model to mimic the heterogeneous tumor microenvironment and to take full advantage of the imaging depth of PAI. Our study setting aligns more with the clinical setting thus reflecting the significance for clinical translation.

In this study, we also demonstrated the depth of penetration advantage of PAI in the rat orthotopic PCa model. Even with a certain distance between the skin and the tumor area, excellent molecular PAI images were obtained successfully for the whole prostate gland. The molecular PAI signal in cRGD-ICG group peaked at a depth of 10 mm, where the orthotopic tumor was located, demonstrating the targeting ability of the probe. In fact, the PAI's depth of penetration is more than 5 cm which meets the basic clinical needs.

In the present study, PAI and US imaging were merged to co-present orthotopic PCa and surrounding anatomical area, including prostate and bladder. This anatomical information is vital not only for avoiding injury to normal tissues during biopsy procedure but also to identify PCa areas in PAI. The merged PAI and US image identified PCa for targeted biopsy, aided by the critically important targeting ability of the molecular probe towards tumor angiogenesis. We quantitatively analyzed the molecular imaging result of PCa in this study. The rats injected with targeted probe showed 3.8 × higher (P < 0.05) PA signal in tumor region compared to those injected with the non-targeted probe, which validates the significant targeting ability of our molecular PAI for PCa. The merged imaging method enabled visualizing and quantifying tumor malignancy at a molecular level and increased the sensitivity of diagnosing the tumor which will potentially increase the accuracy of targeted biopsy and even local treatment for PCa clinically.

Notably, there are some limitations of our study. First, the targeting probe we used in this study to visualize PCa is a general molecule, which overexpresses in a wide range of diseases. While we were successful in clearly identifying the PCa, a probe specifically targeting PCa would be more than welcome. We will investigate such a probe in the near feature. Second, as the diagnosis of androgen-dependent and independent PCa remain a pressing issue, the targeting ability of the molecular PAI should be further explored to address the problem. Third, the development of PA-based multi-modal contrast agents that can provide complementary information from various different imaging modalities is still warranted. In the absence of such a contrast agent, our ICG-based contrast agent is a valuable targeting agent for PCa diagnosis in the multi-modal PAI.

5. Conclusions

In this study, we successfully synthesize an integrin $\alpha_v\beta_3$ targeting PAI probe by combining favorable photoacoustic properties of ICG and the specific $\alpha_v\beta_3$ -binding capabilities (cRGD-ICG). Employed with the cRGD-ICG, molecular PAI showed the excellent diagnosing ability for murine orthotopic PCa models by PAI/US merged imaging. The strategy we developed in this work showed great potential for guiding targeted prostate biopsy towards highly suspicious regions, thus increasing the yield of biopsy rate during the systematic biopsy. Because the dye is already FDA approved and the PAI depth of imaging is more than 5 cm, we believe our study presents a compelling reason to use our system in the real clinical situation. In the near future, we plan to conduct a clinical study in humans.

References

1.
Litwin MS, Tan HJ. The Diagnosis and Treatment of Prostate Cancer: A Review[J]. JAMA. 2017;317(24):2532–42.

2.
Malvezzi M, Bertuccio P, Rosso T, et al. European cancer mortality predictions for the year 2015: does lung cancer have the highest death rate in EU women?[J]. Annals of Oncology Official Journal of the European Society for Medical Oncology. 2015;26(4):779.

3.
Chen W, Zheng R, Baade PD, et al. Cancer statistics in China, 2015[J]. CA: A Cancer Journal for Clinicians, 2016, 66(2):115–132.

4.
Gosselaar C, Roobol MJ, Roemeling S, et al. The value of an additional hypoechoic lesion-directed biopsy core for detecting prostate cancer[J]. BJU Int. 2008;101(6):685–90.

5.
Han M, Chang D, Kim C, et al. Geometric Evaluation of Systematic Transrectal Ultrasound Guided Prostate Biopsy[J]. J Urol. 2012;88(6):2404–9.

6.
Gayet M, van der Aa A, Beerlage HP, et al. The value of magnetic resonance imaging and ultrasonography (MRI/US)-fusion biopsy platforms in prostate cancer detection: a systematic review[J]. BJU Int. 2016;117(3):392–400.

7.
Tempany CM, Turkbey B, Rosenkrantz AB. The Current State of MR Imaging-targeted Biopsy Techniques for Detection of Prostate Cancer[J]. Radiology. 2017;285(2):343–56.

8.
Smeenge M, Tranquart F, Mannaerts CK, et al. First-in-Human Ultrasound Molecular Imaging With a VEGFR2-Specific Ultrasound Molecular Contrast Agent (BR55) in Prostate Cancer[J]. Invest Radiol. 2017;52(7):419–27.

9.

Fanti S, Minozzi S, Antoch G, et al. Consensus on molecular imaging and theranostics in prostate cancer[J]. The Lancet Oncology. 2019;19(12):e696–708.

10.

Wang LV. Multiscale photoacoustic microscopy and computed tomography[J]. Nat Photonics. 2009;3(9):503–9.

11.

Sheng W, Jing L, Tianfu W, et al. Recent Advances in Photoacoustic Imaging for Deep-Tissue Biomedical Applications[J]. Theranostics. 2016;6(13):2394–413.

12.

Stoffels I, Morscher S, Helfrich I, et al. Metastatic status of sentinel lymph nodes in melanoma determined noninvasively with multispectral optoacoustic imaging[J]. Sci Transl Med. 2015;7(317):317ra199.

13.

Xu M, Wang LV. Photoacoustic imaging in biomedicine[J]. Rev Sci Instrum. 2006;77(4):41101–0.

14.

Ni J, Cozzi P, Hung TT, et al. Monitoring Prostate Tumor Growth in an Orthotopic Mouse Model Using Three-Dimensional Ultrasound Imaging Technique[J]. Translational Oncology. 2016;9(1):41–5.

15.

Dijkstra BM, Jeltema HJ, Kruijff S, et al. The application of fluorescence techniques in meningioma surgery—a review[J]. Neurosurg Rev. 2018;2019, 42(4):799–809.

16.

Zheng C, Zheng M, Gong P, et al. Indocyanine green-loaded biodegradable tumor targeting nanoprobes for in vitro and in vivo imaging[J]. Biomaterials. 2012;33(22):5603–9.

17.

Wang H, Liu C, Gong X, et al. In vivo photoacoustic molecular imaging of breast carcinoma with folate receptor-targeted indocyanine green nanoprobes.[J]. Nanoscale. 2014;6(23):14270–9.

18.

Desgrosellier JS, Cheresh DA. Integrins in cancer: biological implications and therapeutic opportunities[J]. Nat Rev Cancer. 2010;10(1):9.

19.

Sipkins DA, Cheresh DA, Kazemi MR, et al. Detection of tumor angiogenesis in vivo by $\alpha_v\beta_3$-targeted magnetic resonance imaging[J]. Nat Med. 1998;4(5):623–6.

20.

Beer AJ, Haubner R, Sarbia M, et al. Positron emission tomography using [18F]Galacto-RGD identifies the level of integrin $\alpha v\beta 3$ expression in man. Clin Cancer Res[J] Clinical Cancer Research. 2006;12(13):3942.

21.

Li M, Liu C, Gong X, et al. Linear array-based real-time photoacoustic imaging system with a compact coaxial excitation handheld probe for noninvasive sentinel lymph node mapping[J]. Biomedical Optics Express. 2018;9(4):1408–22.

22.

Bai Y, Cong B, Gong X, et al. Compact and low-cost handheld quasibright-field linear-array probe design in photoacoustic computed tomography[J]. J Biomed Opt. 2018;23(12):1–10.

23.

Jelena L, Ataya S, Gambhir SS. A high-affinity, high-stability photoacoustic agent for imaging gastrin-releasing peptide receptor in prostate cancer[J]. Clin Cancer Res. 2014;20(14):3721–9.

Declarations

Ethics approval and consent to participate

All animal experiments were approved by the Sun Yat-sen University Animal Care Committee.

Consent for publication

Not applicable.

Availability of data and materials

All data generated or analysed during this study are included in this published article [and its supplementary information files].

Competing interests

The authors declare that they have no competing interests.

Funding

Authors' contributions

C. Q participated in designing the study, did major experiments and wrote paper; TH. Y also designed the study and wrote the paper; YY. B contributed in the photoacoustic experiment and PAI data analysis; XY. M helped with the animal experiment; RK. G also contributed in the photoacoustic experiment; HC. Z helped with the cell experiment; J. R partly designed the study; CB. L and HR. Z supervised the study and edited paper; RQ. Z designed the study and edited paper.

Abbreviations

PCa   prostate cancer

US   ultrasound

TRUS transrectal ultrasound

MpMRI multiparametric Magnetic Resonance Imaging

PAI   Photoacoustic imaging

RGD   arginine-glycine-aspartic acid sequence

cRGD cyclic arginine-glycine-aspartic acid sequence
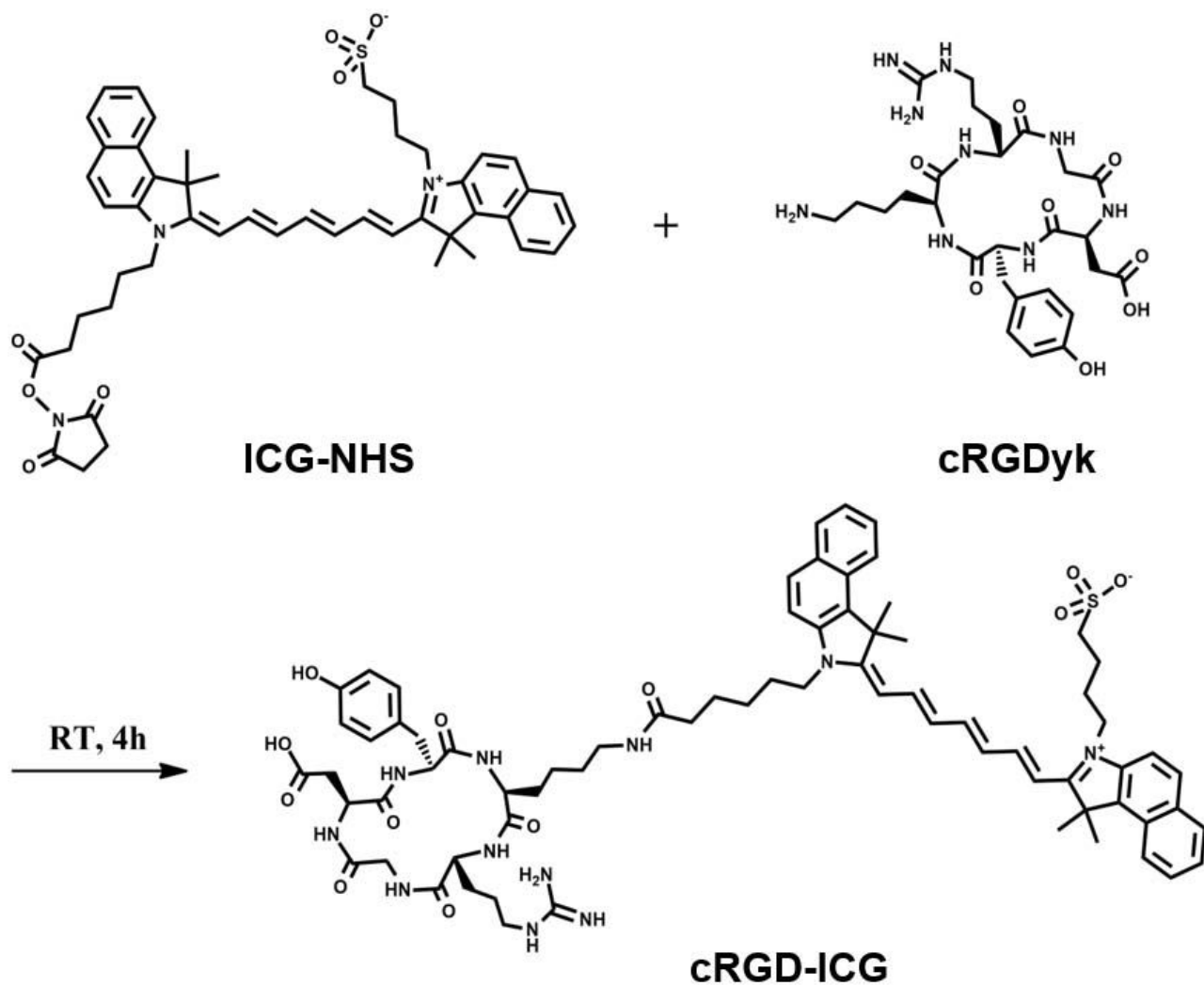
DMSO dimethyl sulfoxide

UV-Vis ultraviolet-visible

HUVEC human umbilical vein endothelial cells
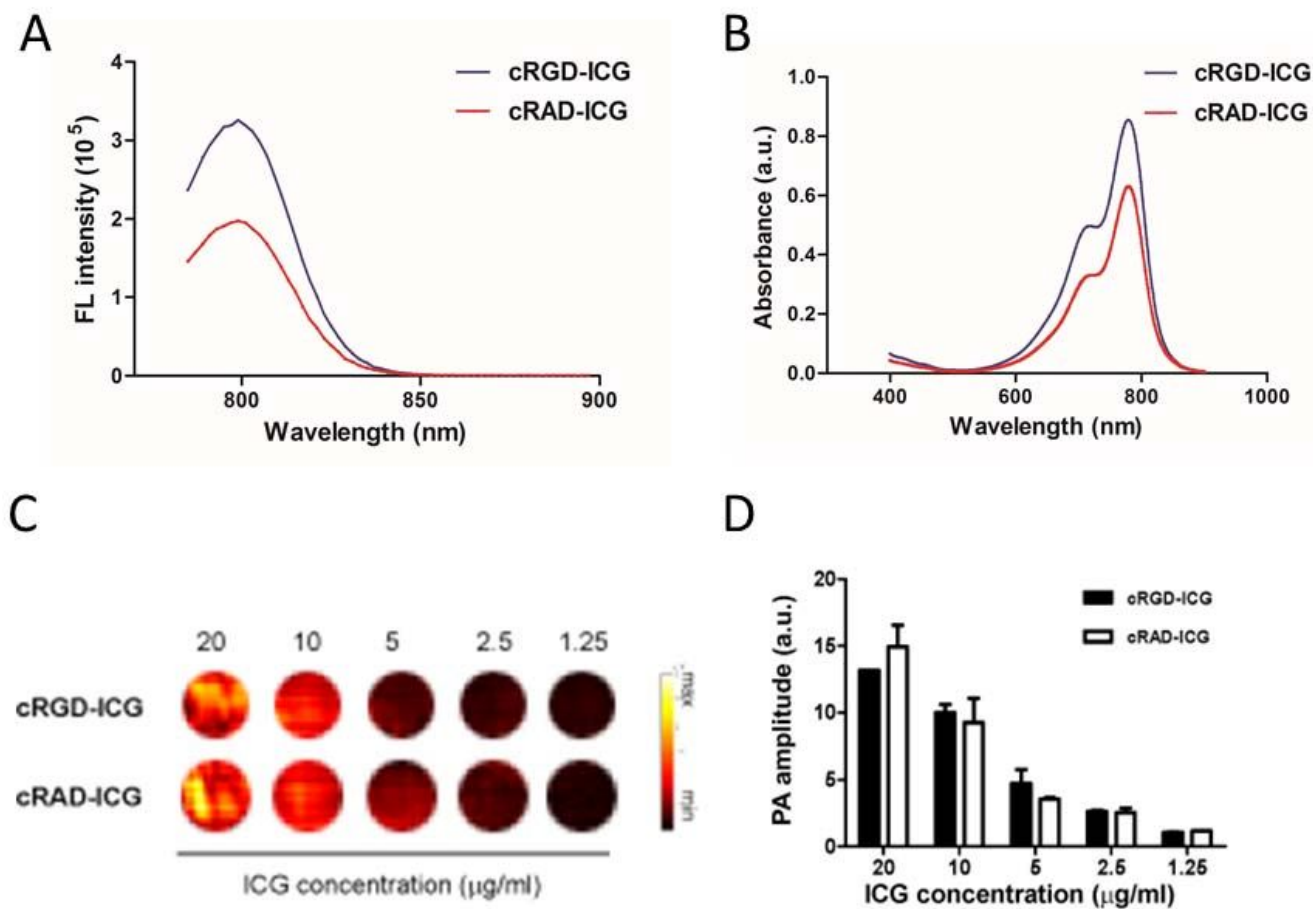
293T   human embryonic kidney cells

FBS   fetal bovine serum

Figures

Figure 1

Schematic structures of ICG conjugated c(RGDyk) probes
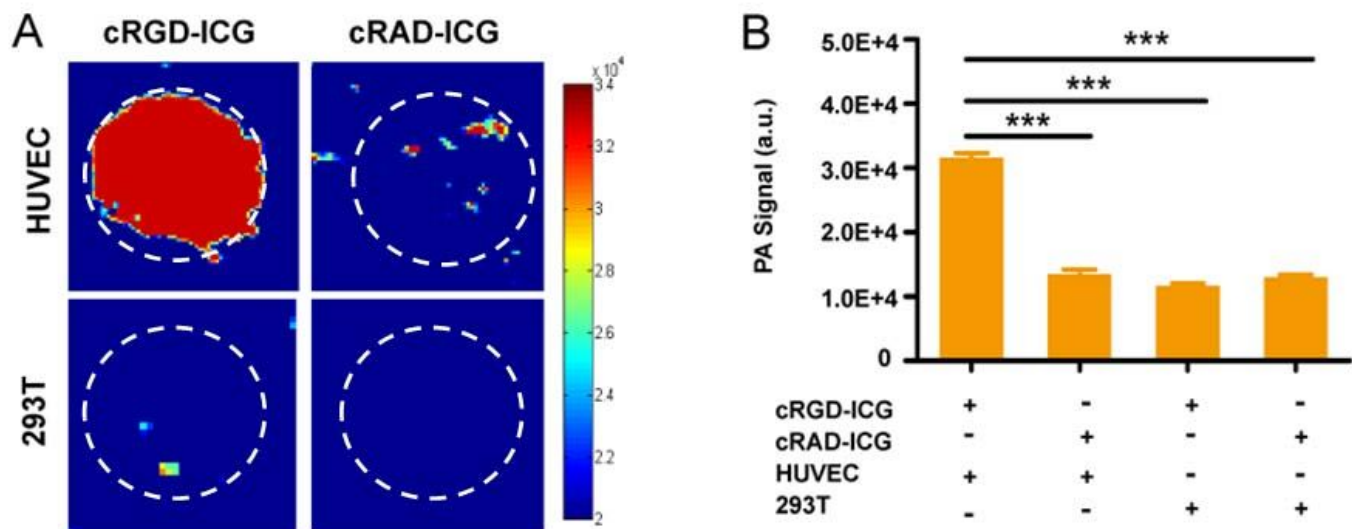
Figure 2

Characterization of cRGD-ICG. (A) Emission spectra of both cRGD-ICG and cRAD-ICG. (B) Absorbance spectra of both cRGD-ICG and cRAD-ICG. (C) In vitro photoacoustic images of cRGD-ICG and cRAD-ICG. (D) In vitro photoacoustic amplitude signal of a series of concentrations cRGD-ICG and cRAD-ICG.
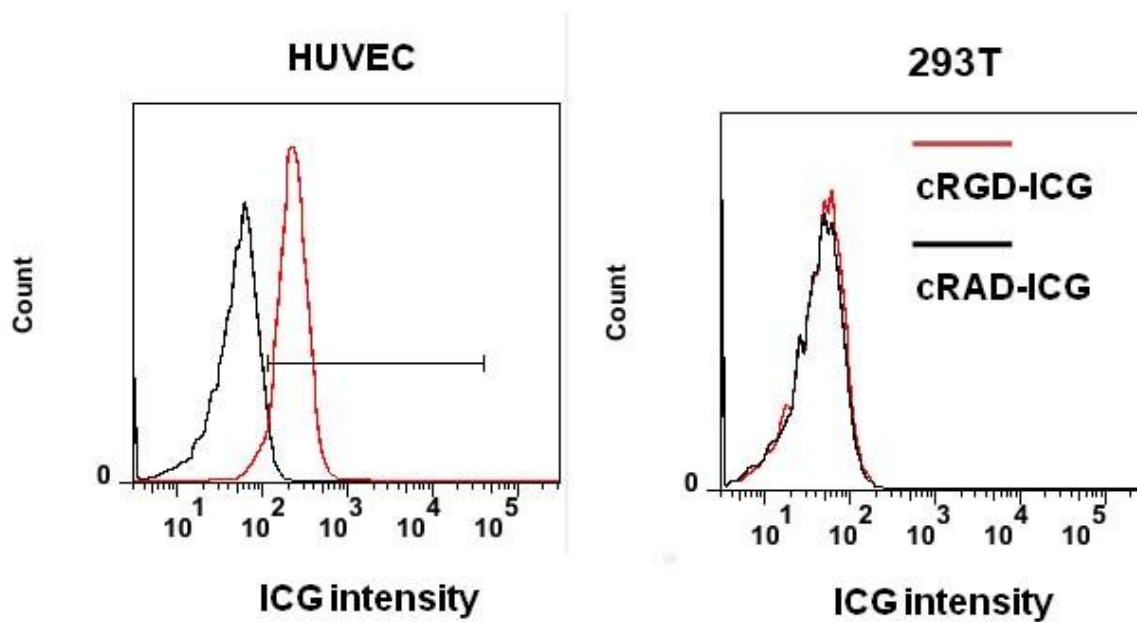
Figure 3

Cell specific uptake of cRGD-ICG by flow cytometry. Red curves: HUVECS or 293T incubated with cRGD-ICG. Black curves: HUVECS or 293T incubated with cRAD-ICG.

Figure 4

Photoacoustic signals of cell inoculation. (A). Cellular photoacoustic images. (B). Cellular photoacoustic amplitude signal analysis.
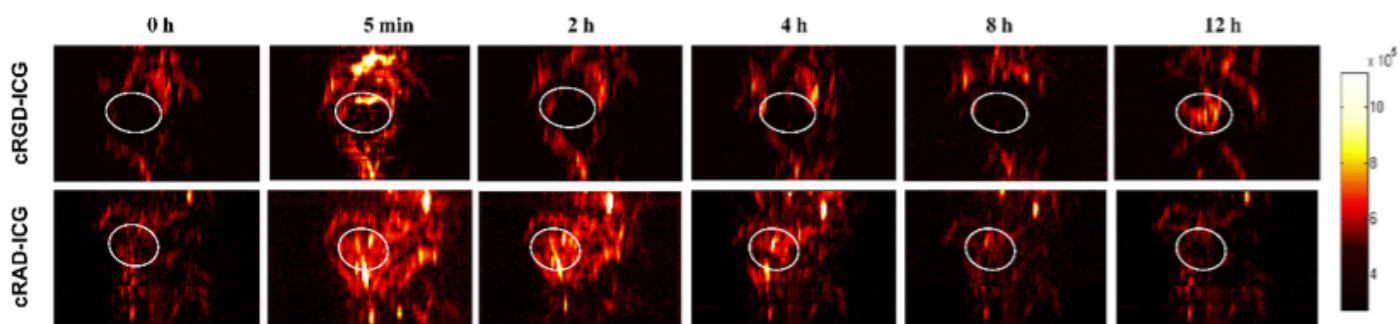
Figure 5

PAI of rats are bearing orthotopic PCa after injected with cRGD-ICG or cRAD-ICG for a period of time. White circle: suspicious tumor area in the prostate.
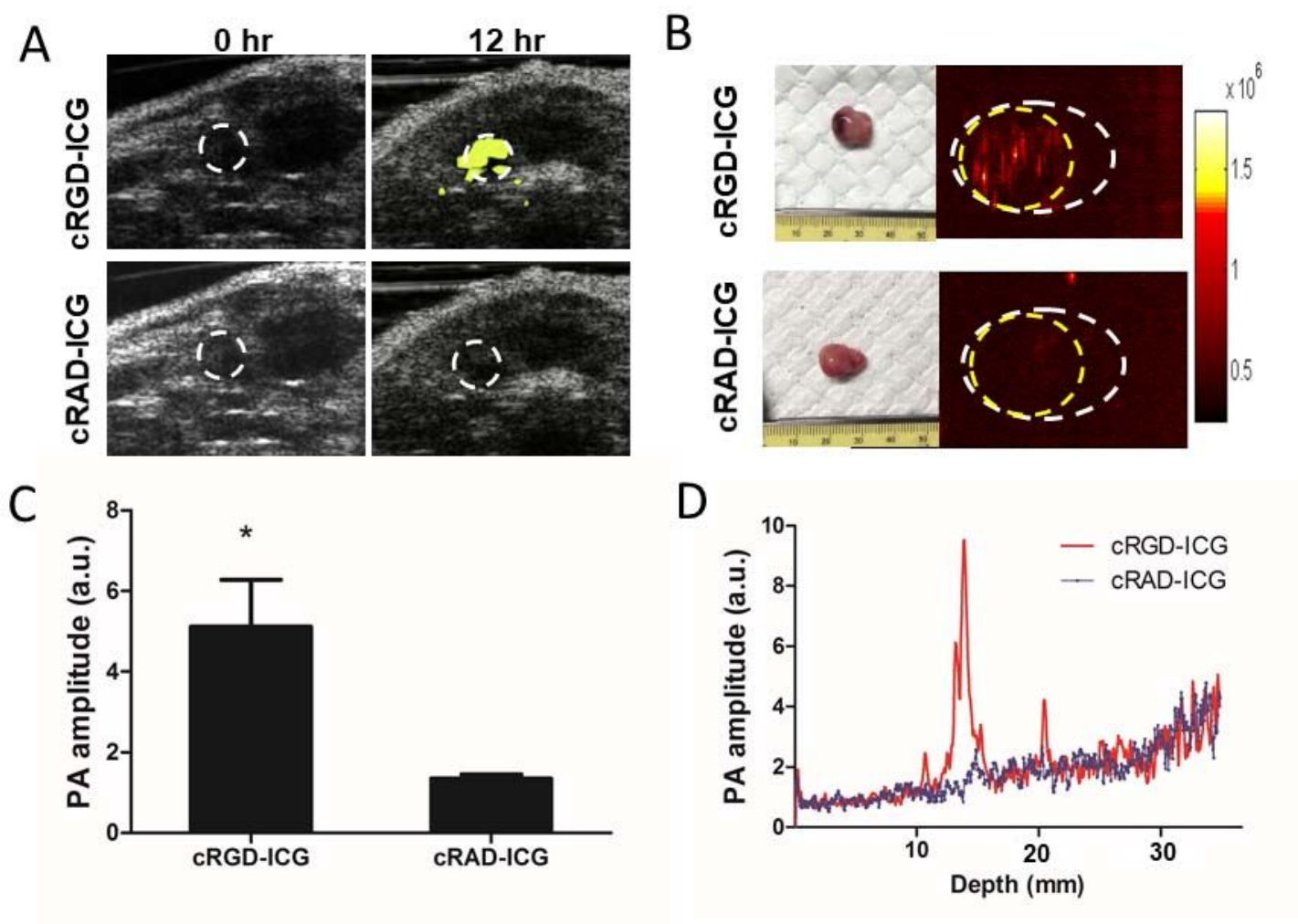

Figure 6

Integrin $\alpha\nu\beta3$ targeted PAI of orthotopic PCa. (A) In vivo integrin $\alpha\nu\beta3$ PAI images merged with US images. (B) Ex vivo PAI images of prostate harvested at 12 h. Yellow circle: tumor area. White circle: the whole

prostate including tumor and normal tissue. (C) PAI signal enhancement after injection with dye. (D) PAI signal varied from depths at 12 h.
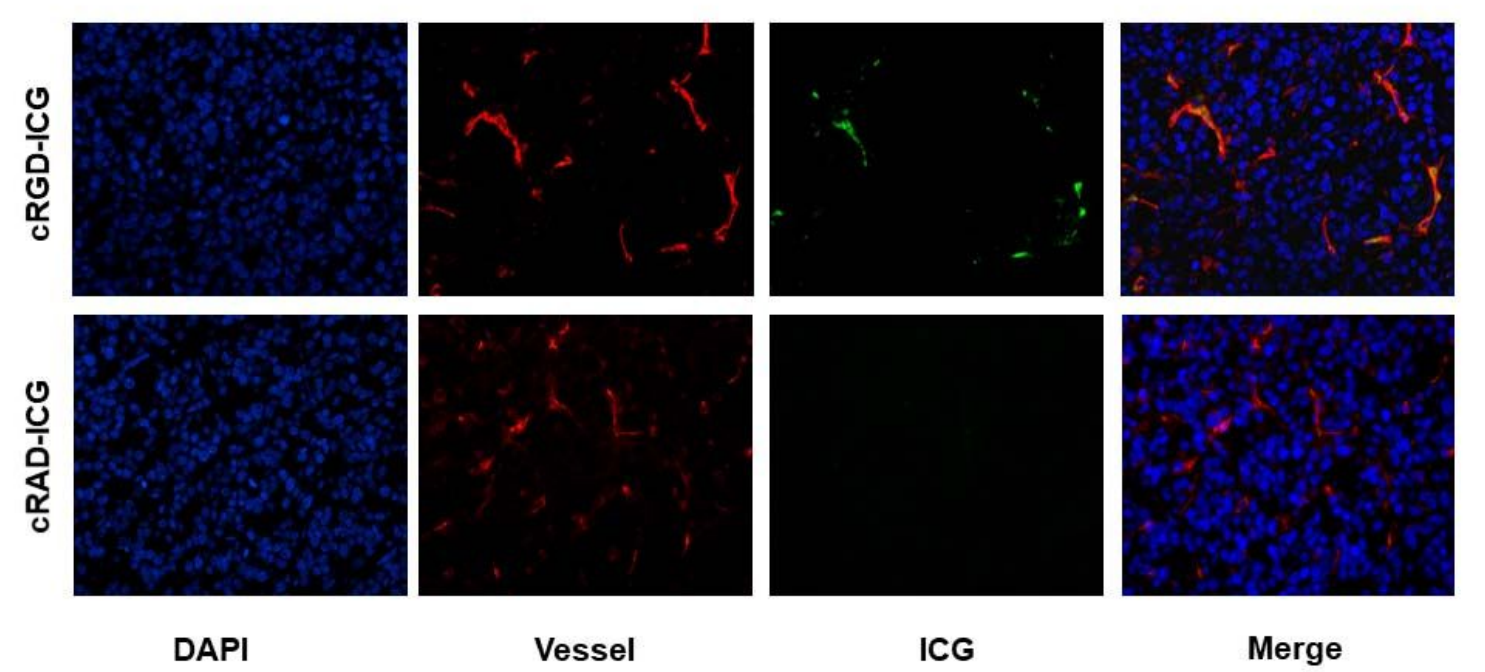

Figure 7

Confocal microscope imaging of ICG in tumor tissue. Blue fluorescence: nuclei stained with Hoechst 33342; Red fluorescent: vessel stained with FITC; Green fluorescent: ICG. (Magnitude: 400 ×)